Elastic constants of defected and amorphous silicon with the environment-dependent interatomic potential

Clark L. Allred,[1,2,3] Xianglong Yuan,[1] Martin Z. Bazant,[4] and Linn W. Hobbs[1,*]
[1]*Department of Materials Science and Engineering, Massachusetts Institute of Technology, Cambridge, Massachusetts 02139, USA*
[2]*The Charles Stark Draper Laboratory, Inc., 555 Technology Square, Cambridge, Massachusetts 02139, USA*
[3]*Air Force Institute of Technology, Wright-Patterson AFB, Ohio 45433, USA*
[4]*Department of Mathematics, Massachusetts Institute of Technology, Cambridge, Massachusetts 02139, USA*
(Received 9 February 2004; revised manuscript received 20 May 2004; published 29 October 2004)

The elastic constants of a wide range of models of defected crystalline and amorphous silicon are calculated, using the environment-dependent interatomic potential (EDIP). The defected crystalline simulation cells contain randomly generated defect distributions. An extensive characterization of point defects is performed, including structure, energy and influence on elastic constants. Three important conclusions are drawn. (1) Defects have independent effects on the elastic constants of silicon up to (at least) a defect concentration of 0.3%. (2) The linear effect of Frenkel pairs on the ⟨110⟩ Young's modulus of silicon is −1653 GPa per defect fraction. (3) 17 different point defect types cause a very similar decrease in the ⟨110⟩ Young's modulus: $-(0.28\pm0.05)\%$ when calculated in isolation using a 1728-atom cell. These principles will be very useful for predicting the effect of radiation damage on the elastic modulus of silicon in the typical case in which point-defect concentrations can be estimated, but the exact distribution and species of defects is unknown. We also study amorphous samples generated in quenching the liquid with EDIP, including an ideal structure of perfect fourfold coordination, samples with threefold and fivefold coordinated defects, one with a nanovoid, and one with an amorphous inclusion in a crystalline matrix. In the last case, a useful finding is that the change in the Young's modulus is simply related to the volume fraction of amorphous material, as has also been observed by experiment.

DOI: 10.1103/PhysRevB.70.134113 PACS number(s): 62.20.Dc, 61.82.−d

I. INTRODUCTION

Defects in silicon have been more extensively studied for their effects on electronic properties than for their effects on mechanical properties. This is not surprising, given the extensive uses that have been made of silicon's electronic properties. With the advent of ever more-sensitive microelectromechanical (MEMS) devices, however, the importance of precise knowledge of the mechanical properties of component materials has grown. Shifts in mechanical properties may well compromise the functioning of a highly sensitive MEMS device. Radiation damage and even small changes in temperature or stress state can cause sufficient alteration of dimension and elasticity to be of concern.

Radiation-induced changes in the mechanical properties of silicon, a common MEMS material, have been studied for rather large ion fluences and elastic constant changes, from $\gtrsim 5\%$ (Ref. 1) to complete amorphization.[2–4] Such high levels of radiation damage are common when performing ion implantation. It is not clear, however, that effects at very low radiation doses, such as might occur in an environment such as space, can be correctly extrapolated from such high-dose regimes. While not simulating radiation damage *per se*, the present study addresses elastic constant changes occurring in defected and amorphous silicon, both possible results of irradiation.

Molecular dynamics simulations predict that radiation damage consists of a mixture of isolated defects, aggregate defects, and amorphous regions.[5–8] Whether the isolated defects or amorphous regions dominate will depend on such factors as the incident particle flux, mass, and energy, as well as the temperature of the damaged material. Heavier, more energetic recoils produce larger amorphous pockets which are unlikely to anneal, even at room temperature.[5] The qualitative results of these studies are relatively insensitive to the interatomic potentials used, among the most popular and well-tested models of silicon: the Stillinger-Weber (SW) potential[9] (Refs. 5, 7, and 8), the Tersoff potentials[10,11] (Refs. 6–8), and the environment-dependent interatomic potential (EDIP)[12,13] (Ref. 8).

For the present study of crystalline defects and amorphous silicon, EDIP is a natural choice. It was fit to a few point defect energies and then tested for a wide variety of unrelated structures, with considerable success in light of its relatively small number of parameters (13). For example, among the most commonly used potentials, EDIP is the only one to correctly predict dislocation core reconstructions and a direct quench from the liquid to a high quality amorphous phase.[13] Since the original study, EDIP has been used extensively in simulations of crystalline defects[14–19] and amorphous structures,[20–25] so it may be considered well tested for the present application.

More importantly, from a physical point of view, EDIP includes environment-dependent changes in chemical bonding, inferred directly from *ab initio* calculations and experimental data.[12,26,27] Specifically, the bond order (strength of the pairwise attraction), the preferred bond angle, and the angular stiffness depend strongly on the local coordination number *Z*. In contrast, the form of the SW potential can only be justified for rigid sp^3 hybrid bonds, which, in reality, are

Report Documentation Page

Form Approved
OMB No. 0704-0188

1. REPORT DATE	2. REPORT TYPE	3. DATES COVERED
20 MAY 2004		**00-00-2004 to 00-00-2004**

4. TITLE AND SUBTITLE	5a. CONTRACT NUMBER
Elastic constants of defected and amorphous silicon with the environment-dependent interatomic potential	5b. GRANT NUMBER
	5c. PROGRAM ELEMENT NUMBER
6. AUTHOR(S)	5d. PROJECT NUMBER
	5e. TASK NUMBER
	5f. WORK UNIT NUMBER
7. PERFORMING ORGANIZATION NAME(S) AND ADDRESS(ES) **Air Force Institute of Technology,Wright-Patterson AFB,OH,45433**	8. PERFORMING ORGANIZATION REPORT NUMBER
9. SPONSORING/MONITORING AGENCY NAME(S) AND ADDRESS(ES)	10. SPONSOR/MONITOR'S ACRONYM(S)
	11. SPONSOR/MONITOR'S REPORT NUMBER(S)

12. DISTRIBUTION/AVAILABILITY STATEMENT
Approved for public release; distribution unlimited

13. SUPPLEMENTARY NOTES

14. ABSTRACT

15. SUBJECT TERMS

16. SECURITY CLASSIFICATION OF:			17. LIMITATION OF ABSTRACT	18. NUMBER OF PAGES	19a. NAME OF RESPONSIBLE PERSON
a. REPORT **unclassified**	b. ABSTRACT **unclassified**	c. THIS PAGE **unclassified**	**Same as Report (SAR)**	**13**	

replaced by other covalent hybrids or metallic bonds in nontetrahedral defects and disordered structures.[12,26] The reasonable description of the metallic liquid and certain defects by SW, therefore, should be viewed as fortuitous. In comparison, the Tersoff potentials incorporate more realistic features of the bond order, which can be derived analytically from tight-binding models.[28] The functional form, however, is inconsistent with silicon elastic constant relations[12] (satisfied by SW and EDIP) and seems unable to simulataneously describe elasticity, defects, and phase transitions.[29]

The importance of the choice of potential is well illustrated by the present topic. Experiments and simulations both show that amorphous silicon is less stiff than the crystal.[2,3,30,31] On the other hand, the only prior work on the effect of defects at low concentrations on crystal elasticity by Clark and Ackland (CA) concludes that both vacancies and interstitials tend to increase the elastic constants,[32] although one might expect the opposite trend, since the accumulated effect of defects in the crystal roughly approaches an amorphous structure. These authors introduced a new potential depending only upon pairwise bond lengths, which has since received very little testing. A serious concern regarding their results is the poor description of the crystal elastic constants by the CA potential (compared to SW and EDIP), which can be attributed to the lack of explicit angular dependence, in violation of silicon elastic constant relations[12] and analysis of tight-binding models.[28,33] Following Ackland,[34,35] the CA potential also assumes exactly four bonds per atom, which obviously cannot apply to most defects. Therefore, it is not surprising that in the present study with EDIP we reach a very different conclusion: point defects tend to make the crystal more soft (as is the amorphous phase). We check that the same trend is predicted by SW, so it is clear that angular terms, neglected by CA, play an important role.

In practical situations, it is the finite-temperature behavior of silicon elasticity that would be of interest. While statistical mechanical methods do exist for calculating finite-temperature elastic constants (e.g., Monte Carlo[36] or molecular dynamics[37] simulations), we decided not to pursue such methods in this study. We justify this choice in light of the small defect fractions and concurrently small shifts in elastic constant that were considered here, which would have been difficult to notice with the slower convergence of fluctuation methods. In addition to having greater precision, the cell deformations described below were much simpler and computationally cheaper than finite-temperature methods. Since the elastic constants of silicon shift only by around 1% between 0 and 300 K,[38] we believe that the trends in the elastic constants with defect content are essentially captured by our zero-temperature calculations.

II. METHODS

A. Sample creation

1. Defected samples

Defected samples were created by inserting vacancies and interstitials into 1728-atom supercells ($6\times6\times6$ unit cells), using periodic boundary conditions. Randomly selected atoms were removed to produce vacancies and random positions were chosen to insert extra atoms. Three types of sample were produced: one containing only vacancies, one having only interstitials, and one containing Frenkel pairs. Fifteen samples were produced of each sample type, consisting of three sets of supercells containing 1,2,3,4, and 5 defects, for a grand total of 45 sample supercells.

Upon insertion of defects, the supercells were relaxed at 0 K by relaxing atomic positions while iterating over cell dimension changes. Isotropic expansion and cell-length changes along individual axes were iteratively explored following a simple energy gradient algorithm. The supercells were then annealed at 300 K for 500 ps using the DL_POLY (Ref. 39) NPT ensemble with Berendsen thermostat and barostat. After annealing, the supercells were again relaxed at 0 K.

It was hoped that this procedure would yield samples representing several different defect types in random geometries, as might result in regions of a collision cascade rich in point defects. Some samples were thrown out and regenerated, since sometimes a randomly chosen vacancy and a randomly placed extra atom annihlated either immediately or upon annealing. Other times, a randomly chosen position for an extra atom was too close to a crytalline position in the supercell, and mayhem resulted upon relaxation due to the large forces present. Samples were visually inspected to ensure that the desired scattered defects were present and discernably distinct. In most cases, only isolated defects were present. Exceptions included a two-interstitial agglomerate (H_2), and divacancy complexes involving missing nearest neighbors (V_{2N}) and missing next-nearest neighbors (V_{2NN}). A breaking of symmetry in the (V_{2NN}) complex yielded another divacancy type (V_{2a}).

In addition to these 45 defected samples, 17 additional 1728-atom supercells were prepared in order to characterize the formation energy (E_f), volume (V_f), and effects on elastic constants of various interstitial and vacancy configurations. These samples were created by intentionally arranging atomic positions within the supercell then relaxing at 0 K, as above. E_f, V_f, and elastic constants for each sample were calculated before annealing the sample at 300 K for 500 ps, as above. Calculations were then repeated on the annealed samples.

2. Amorphous samples

Brief descriptions of the defect content of amorphous samples are given in Table I. Amorphous samples A, D, and G were prepared by quenching from the liquid at zero pressure as follows. A diamond crystal was melted at 3000 K for 50 ps, cooled to 1500 K over 100 ps, then equilibrated at 1500 K for an additional 100 ps. The samples were then cooled 1000 K over 1 ns (the transition from liquid to the amorphous state occurred at this step), then annealed at 1000 K for 2 ns. The annealed amorphous sample was then cooled to 0 K over 2 ns.

Amorphous samples B and C were derived from an intermediate sample that was prepared from sample A as follows. A negative pressure of −100 GPa was imposed on sample A at 0 K, then the sample was annealed at 1000 K for 2 ns and

TABLE I. Descriptions of amorphous samples. Calculation of numbers of fivefold and threefold coordination defects present used a rounding of the EDIP coordination value *Z*.

Sample	Size	Fivefold	Threefold	Other
A	216	6	0	
B	216	5	1	
C	216	13	3	Void present
D	216	10	0	
E	1728	116	2	
F	1728	112	2	
G	64	0	0	

slowly cooled to 0 K at constant volume. Finally, the structure was relaxed to zero pressure.

Sample B was derived from this intermediate structure by annealing at 1100 K for 2 ns and cooling to 0 K, all at zero pressure. Sample C was derived from the same intermediate structure by annealing at 1100 K for 4 ns and then cooling to 0 K, all at constant volume. The defect content of sample B was similar to that of sample A, whereas sample C contained a sizable void.

Two 1728-atom amorphous samples were prepared by quenching from high temperature at constant pressure. Sample E was prepared by heating a crystalline sample to 3000 K, equilibrating for 300 ps, then cooling to 10 K at 1 K/ps. Sample F started with random atomic positions at 5000 K, then was cooled to 10 K, also at 1 K/ps. All amorphous samples used here were annealed at 300 K for 500 ps, then relaxed at 0 K as for the defected samples above.

3. Amorphous pocket sample

A composite sample consisting of an amorphous block surrounded by crytalline material was prepared by embedding sample G into a crystalline matrix. This was done by first cutting out a $2\times2\times2$ unit cell cube from a $6\times6\times6$ unit cell supercell. The crystalline supercell was then homogeneously and anisotropically expanded to accommodate the relaxed sample G. The sample containing the amorphous pocket was then relaxed at 0 K as above, then annealed as above at 300 K and relaxed again at 0K.

B. Elastic constant calculation

1. Approach

Strain can be defined as[40]

$$\epsilon_{ij} = \tfrac{1}{2}(e_{ij} + e_{ji}), \tag{1}$$

where

$$e_{ij} = \frac{\partial u_i}{\partial x_j}, \tag{2}$$

with u being displacement and x being position. The work needed to impose a strain ϵ is (switching to Voigt notation)

$$\frac{\Delta E}{V} = \frac{1}{2} C_{ij}\epsilon_i\epsilon_j, \tag{3}$$

where C_{ij} are the elastic constants and V is the volume. For a cubic system such as silicon, only three independent constants exist. We make the approximation for our defected samples that this symmetry remains intact.

Computationally convenient strains to impose on an orthorhombic supercell aligned with the diamond unit cell axes are suggested by Eq. (3). The tensor strain notation shown in Eq. (4) is used in Eqs. (5)–(7), with nonspecified strains all equal to zero:

$$\epsilon = \begin{bmatrix} \epsilon_1 & \frac{1}{2}\epsilon_6 & \frac{1}{2}\epsilon_5 \\ \frac{1}{2}\epsilon_6 & \epsilon_2 & \frac{1}{2}\epsilon_4 \\ \frac{1}{2}\epsilon_5 & \frac{1}{2}\epsilon_4 & \epsilon_3 \end{bmatrix}, \tag{4}$$

TABLE II. Analytical and numerically (energy curve fitting) computed EDIP elastic constants (GPa) and Kleinman's internal strain parameter ζ for the diamond phase. C_{44}^0 is the shear modulus when internal relaxation is disallowed. The values published by Justo *et al.* are provided here for comparison.

	Analytical	Numerical	Justo *et al.* (Ref. 13)	Expt. (Refs. 38 and 41)
C_{11}	171.99	172.00	175	167.54
C_{12}	64.72	64.71	62	64.92
C_{44}	72.75	72.75	71	80.24
C_{44}^0	112.39	112.39	112	111[d]
B	100.47	100.47	99	99.13
ζ	0.51727	0.51727[a]	0.497[b]	0.72
$E_{\langle100\rangle}$[c]	136.60	136.62	143	131.28
$E_{\langle110\rangle}$[c]	164.05	164.05	164	170.63

[a]Calculated computationally by shearing a supercell and measuring atomic relaxation.
[b]Calculated from C_{ij} (Ref. 27).
[c]Calculated from C_{ij} (Ref. 40).
[d]Not experimentally accessible. Calculated using *ab initio* (LDA) methods in Ref. 12.

$$C_{11} = \frac{1}{V}\frac{\partial^2 E}{\partial \epsilon_1^2}, \tag{5}$$

$$C_{11} + C_{12} = \frac{1}{2V}\frac{\partial^2 E}{\partial \epsilon^2}, \ \epsilon = \epsilon_1 = \epsilon_2, \tag{6}$$

$$C_{44} = \frac{1}{V}\frac{\partial^2 E}{\partial \epsilon_4^2}. \tag{7}$$

By imposing isotropic strains ($\epsilon_1 = \epsilon_2 = \epsilon_3$), we can also obtain the bulk modulus

$$B = V\frac{\partial^2 E}{\partial V^2}. \tag{8}$$

2. Defected samples

Elastic constants were calculated by fitting polynomials to plots of energy vs strain. Excellent results were obtained for a wide range of energy sampling intervals in strain for the crystal and for samples containing only point defects, but the amorphous samples were found to be apt to change bonding structure with large imposed strains. By trial and error, it was determined that a step size in strain of 1×10^{-5} was sufficiently small to not cause bonding rearrangements in the amorphous samples, yet produced large enough energy differences to numerically extract second derivatives from fit polynomials.

The number of points to fit was also decided by experimentation. The second deriviative of the energy was of primary concern here. A greater number of points would help to recognize and account for higher-order effects, but a large number of points at large strains would also allow higher-order effects to dominate the fit. A total of 21 points in the strain interval $\pm1\times10^{-4}$ was calculated for each sample discussed here, but it was found that fitting only the nine middle points yielded the most consistent results.

Starting from the relaxed structure, strains were sequentially imposed in steps of 1×10^{-5}. Atomic positions were relaxed at each strain step. Starting again from zero strain, negative strain was then incrementally imposed. Fourth and fifth order fits to the resultant curves were found to give essentially identical results, with lower-order fits giving slightly different results, and higher-order fits being numerically unreliable. All results reported here are based on fourth-order least-squares fits.

To help minimize the error in our assumption that cubic symmetry holds for the defected samples, all C_{ij} were independently calculated for all three orthogonal directions, then averaged. The variation of C_{44} among the three directions was greatest, and rose to $\sim$1% for a few of the samples, but was typically similar to that of C_{11} and C_{12}, namely, $\lesssim$0.1%. The lesser precision of C_{44} is to be expected, given the sample preparation method described in Sec. II A 1, which guarantees that the relaxed sample will occupy an energy minimum with respect to the isotropic and monoaxial expansions used to obtain energy curves for B and C_{11}, but will not guarantee this for the shear applied to calculate C_{44}.

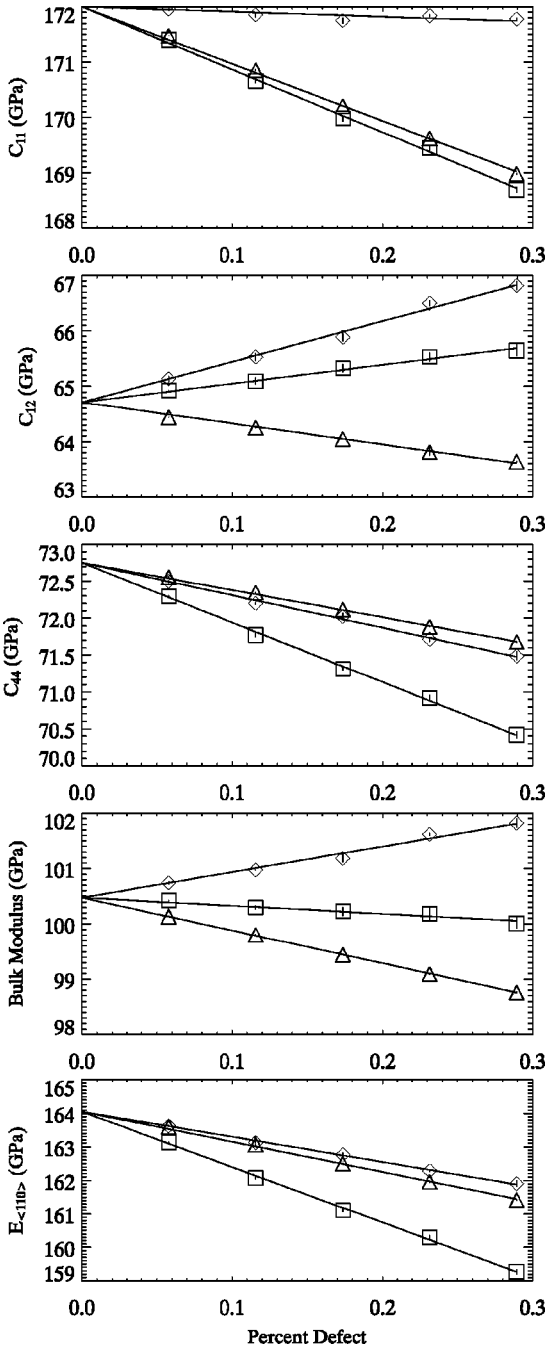

FIG. 1. Elastic constants as a function of point defect fraction. Diamonds indicate interstitials, triangles vacancies, and squares Frenkel pairs. Each point represents the average of three samples. Bars indicate the standard deviation of the three samples. Lines are unweighted least squares fits constrained to match the crystalline value on the Y axis.

As a validation of our numerical approach, we compared values found for the crystal with those previously published for EDIP.[13] When discrepancies were observed, we calculated analytical values[27] for the EDIP diamond lattice elastic constants, and found that our numerically calculated values agreed to within about four significant figures. The results for these values are shown in Table II. It can be seen that the values of Justo *et al.*, calculated using a deformation/energy

TABLE III. Fit slopes to the points in Figs. 1 and 2. Units are per defect fraction, with elastic constants in GPa. "Difference" refers to that between the Frenkel pair result and the sum of the vacancy and interstitial results. The numbers in parentheses are from fits to the data in Clark and Ackland (Ref. 32).

	C_{11}	C_{12}	C_{44}	B	$E_{\langle 110\rangle}$	$\Delta V/V$
Vacancies	−1030(821)	−381(565)	−369(−8.7)	−593(648)	−899(217)	0.42
Interstitials	−89.2(715)	733(443)	−440(−57.9)	462(531)	−751(161)	1.35
Frenkel pairs	−1133	339	−809	−145	−1653	1.78
Vac.+Int.	−1119	352	−810	−130	−1651	1.77
% Difference	−1.2	3.6	0.1	−10.3	−0.2	−0.9

method, very similar to our results in the "numerical" column of Table II, were not accurate to the number of places published. They should be disregarded. Details on calculating the analytical elastic constants from the potential are given in Ref. 27.

3. Amorphous samples

In the case of a truly amorphous material, the elastic properties will be isotropic, and only two independent elastic constants will exist. The finite size and periodic boundary conditions imposed on the samples of our study prohibit this isotropic ideal. We nevertheless calculated the C_{ij} for our amorphous Si samples as above, averaging over results from three independent directions.

An additional step we applied to the amorphous sample elastic constant results was to distill the set of four elastic constants to a self-consistent set by means of an iterative process. The bulk modulus, being direction-independent, was left alone. By pairing each of the three C_{ij} with B, a prediction of the other two C_{ij}'s was made. At each iteration, the original C_{ij} was averaged with the two predicted values until a self-consistent set was achieved. For the largest samples, the change in the C_{ij}'s due to this process was $\lesssim 0.1\%$ for C_{11} and C_{12}, and about 0.5% for C_{44}. For the smallest samples, these changes were ~ 1 and $\sim 10\,\%$, respectively. The small adjustments necessary to achieve self-consistency of the large (1728 atoms) samples demonstrates their close approximation to the isotropic ideal.

4. Amorphous pocket sample

One of the goals of our work was to see what effect amorphous regions embedded in a crystalline matrix (as might be residual from a collision cascade) would have on the overall elastic modulus. As for the defected samples, cubic symmetry doesn't strictly apply for the amorphous pocket sample studied here, nor is the sample isotropic. We wish nevertheless to compare the elastic modulus of the composite with that of its component parts (crystalline and amorphous). We therefore calculated the C_{ij}'s of the composite as for the defected samples. We then reduced the crystalline and composite C_{ij}'s to an effective isotropic Young's modulus E by using the mean of the Reuss and Voigt spatial-average limits.[42]

For isotropic materials, upper and lower bounds on the Young's modulus of a two-phase composite (E_c) are given by[4,43]

$$\left[\frac{V_1}{E_1}+\frac{(1-V_1)}{E_2}\right]^{-1} < E_c < V_1E_1+(1-V_1)E_2, \qquad (9)$$

where V_1 and E_1 are, respectively, the volume fraction and Young's modulus of the embedded material, and E_2 is the Young's modulus of the matrix. Clearly, the crystalline matrix we had here is not isotropic, but the Reuss and Voigt limits for polycrystalline aggregates provide a convenient way to test the applicability of Eq. (9) to our embedded amorphous Si sample.

III. RESULTS

A. Defected samples

The results of the elastic constant calculations for the samples generated by random placement of vacancies and interstitials are summarized in Fig. 1. It can be seen that the trend of the elastic constants with defect content is approximately linear. An unweighted fit was used, since the small standard deviation of the single defect samples, as well as the small number of samples, made weighted fitting difficult to interpret. The fit slopes are summarized in Table III.

The isolated defects appear to be having largely independent effects on the elastic constants and volume, as evidenced by the linear trends in Figs. 1 and 2, as well as by the close agreement between the slope of the Frenkel pair plots and the sum of the vacancy and interstitial slopes as shown in Table III. Both interstitials and vacancies are shown to cause volume expansion in Fig. 2, vacancies to a lesser degree than interstitials. The general softening of the elastic constants with rising defect concentration (with the exception of interstitials for C_{12} and the bulk modulus, and Frenkel

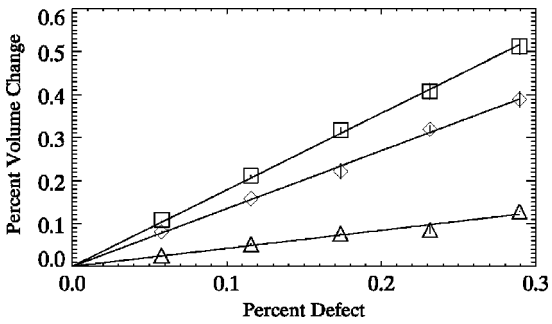

FIG. 2. Percent volume change as a function of point defect fraction. Symbols are as in Fig. 1.

TABLE IV. Elastic constants (GPa) of EDIP-generated amorphous samples described in the text. Also shown are percent volume change and energy gain per atom with respect to the crystalline values (20.018 Å^3 atomic volume and −4.6500 eV). Results from experiment (room temperature), tight-binding molecular dynamics (room temperature), and EDIP are shown for comparison. Where published results were not completely consistent with isotropicity, the range of possible derived values is given.

	C_{11}	C_{12}	C_{44}	B	E	% ΔV	ΔE, eV
A	131.3	80.4	25.5	97.4	70.3	3.8	0.1885
B	130.2	82.9	23.6	98.7	65.7	4.4	0.1999
C (void)	98.7	57.9	20.4	71.5	55.9	10.9	0.2432
D	134.7	82.7	26.0	100.0	71.7	3.3	0.1868
E	133.0	81.9	25.5	99.0	70.5	3.1	0.2059
F	132.9	81.1	25.9	98.4	71.4	3.3	0.2064
G (defect free)	131.0	81.4	24.8	97.9	68.6	5.2	0.1815
EDIP (Ref. 49)	130	81	56	97	67–145	2	0.199
EDIP quench (Ref. 8)						3.5	0.25
EDIP irradiated (Ref. 8)						2.2–3.6	0.19–0.40
Expt. (Ref. 45)[a]	156	58.4	48.8	90.9	124		
Expt. (Ref. 2)	156	57.8	49.2	90.6	125	1.3	
Expt. (Ref. 3)	138	42	48	74	118		
TBMD (Ref. 45)	149	46.9	55.4	75–84	127–136		
Expt. (Ref. 44)						1.8	

[a]The values for C_{ij} here are based on the measured Young's modulus of Tan *et al.* (Ref. 31) combined with a Raleigh wave measurement discussed in De Sandre *et al.* (Refs. 45–48).

pairs for C_{12}) does not agree with the previous finding that both interstitials and vacancies in silicon stiffen the crystal. Vacancies are found here to soften each of the elastic constants considered, the opposite being true for all but C_{44} according to Clark and Ackland.[32] Points of agreement between that study and the present one include the softening of C_{44} by both vacancies and interstitials (though the effect is an order of magnitude greater here), and the stiffening of both B and C_{12} by interstitials.

B. Amorphous samples

Elastic constants of our amorphous samples are shown in Table IV, along with experimental[2,3,31,44–48] and calculated[8,45,49] data for comparison. It can be seen that the differences among samples is slight, with the exception of sample C, which contained a void. The elastic constants for our amorphous samples appear to be fairly insensitive to the coordination defects described in Table I. None of elastic constants of sample G, which has perfect four-coordination throughout, is an outlier when compared to the other samples. Not surprisingly, sample G is the lowest energy configuration. It is interesting to note, however, that the volume change of sample G is the greatest of all EDIP samples reported in Table IV (with the exception, of course, of sample C).

We note that depsite close agreement of our large amorphous samples with the amorphous sample of Vink *et al.*[49] for the values of C_{11} and C_{12}, our value for C_{44} is about a factor of 2 different. As mentioned above, our large (1728 atoms) amorphous samples came very close to satisfying the isotropic ideal represented by

$$C_{44} = \tfrac{1}{2}(C_{11} - C_{12}). \tag{10}$$

Since even our smallest (64 atoms) samples came within 10% of satisfying Eq. (10), with all larger samples being even closer than this (even sample C with its void), one would expect the 1000 atom sample of Vink *et al.* to exhibit fairly isotropic properties. Clearly, the result of Vink *et al.* for C_{44} cannot be correct, since it does not agree with C_{11} and C_{12} according to Eq. (10). We suggest that a factor of two error might have been introduced when calculating C_{44}, which would mean that the actual C_{44} of the Vink *et al.* amorphous sample should be 28 GPa, closer to the 32 GPa that Vink *et al.* report for the amorphous silicon modeled using the Stillinger-Weber potential.[49]

Although the bulk modulus is correctly predicted to be very close to that of the crystal, the overall description of amorphous elasticity is not completely satisfactory. Despite the fact that amorphous samples, both real and computational, have properties that vary according to the method of preparation,[8] it seems likely from the results in Table IV that EDIP errs systematically in predicting the elastic constants of amorphous silicon. All of the experimental studies cited here agree well on the value of C_{44}, and using EDIP to generate and calculate the elastic constants of amorphous samples yields a result consistently about a factor of 2 below this value. This may be related to EDIP's neglect of rehydridization for strains small enough not to change the coordination, which is also responsible for EDIP's underestimation of the Kleinman parameter and the relaxed C_{44} of the crystal.[12] For small distortions of the diamond lattice ($Z=4$), EDIP and SW are both equivalent to the rigid hybrid approximation, which

TABLE V. Elastic constants for the crystal, amorphous sample G, and the amorphous pocket composite sample. The Young's modulus value (E) given for the crystal and the amorphous pocket sample are the average of the Reuss and Voigt spatial averages (Ref. 42). Upper and lower bounds based on Eq. (9) are shown for comparison.

	C_{11}	C_{12}	C_{44}	E
Crystal	172	64.7	72.8	159
Amorphous G	131	81.4	24.8	68.6
Composite	169	65.4	69.9	154
Upper bound				156
Lower bound				151

is very accurate for unrelaxed crystal elasticity, but breaks down with internal relaxation.[27]

C. Amorphous pocket sample

The elastic constants of our amorphous pocket sample are shown (along with those of the component parts) in Table V. It can be seen that the Young's modulus of the composite is within the upper and lower bounds predicted by Eq. (9). This was true, in fact, for all of several different methods we used for applying Eq. (9), including using the Young's modulus for ⟨100⟩ and ⟨110⟩ directions (as opposed to using spatially averaged values). This result agrees with experimental observations of the elastic properties of silicon during amorphization.[4]

Predictions based on Eq. (9) did not hold, however, for elastic constants calculated using a similarly prepared composite sample that skipped the annealing step. The crystalline-amorphous interface, when only relaxed at 0 K, seems the likely reason for this.

D. Isolated defects

The interstitial defects that resulted from the random-placement generation process described in Sec. II A 1 are illustrated in Fig. 3. It can be seen that the defects DB_1, DB_2, and DB_3 are minor variations on the ⟨110⟩ dumbell (DB) defect. In each case, the atom positions are very similar, but sufficiently different to cause the bonding geometry to change. All of these configurations relaxed to the ⟨110⟩ dumbell configuration upon annealing the isolated defect at room temperature. We infer that these defects were stabilized by the presence of other defects.

The DB_4 defect complex is also a variation on the ⟨110⟩ dumbell in which two neighbors of the atom that is "split" to form the dumbell are moved together to bond. While the other dumbell variations may simply be EDIP artifacts, this defect has been seen before with the Tersoff 3 potential.[50]

The formation energy of 3.38 eV calculated for the ⟨110⟩ dumbell defect does not precisely agree with one (3.35 eV) previously published.[13] This is perhaps partly due to our independent relaxation of all three cell dimensions in addition to atomic coordinates, as well as to size effects with periodic boundary conditions, as suggested by Fig. 4. Effects of an overlapping strain field due to periodic boundary conditions don't appear to be of concern (at least to the level of precision discussed here) for our 1728 atom samples. While we did not verify this for each of the many samples discussed in the present work, we take confidence in the leveling off of the curve in Fig. 4.

We calculated the unrelaxed formation energies of the tetragonal and hexagonal interstitials for EDIP, and obtained 10.58 and 6.85 eV, respectively, in agreement with Justo *et al.* We noted, however, that these two interstitial positions are not stable in EDIP, as shown in Fig. 5. An interstitial will shift away from these positions upon relaxation. In fact, even at 0 K, numerical error generated during the relaxation of atomic positions provided sufficient asymmetry to cause the hexagonal interstitial to relax into an off-center position (hex_A). This asymmetric position remains sixfold coordinated. To obtain a relaxed formation energy for the hexagonal interstitial, therefore, the interstitial position had to be artificially maintained. This relaxed configuration for the hexagonal defect was metastable, with a formation energy of 4.19 eV. After room-temperature annealing, both hexagonal and tetragonal interstitials relaxed into a ⟨110⟩ dumbell. This instability of the tetrahedral interstitial agrees with LDA predictions.[51] The result that the unrelaxed hexagonal interstitial is unstable, but that relaxing the system while constraining symmetry among its neighbors yields a metastable defect, also agrees with the *ab initio* result.[52]

We also note in passing that a bond defect involving no coordination defects is stable using EDIP, the relaxed forma-

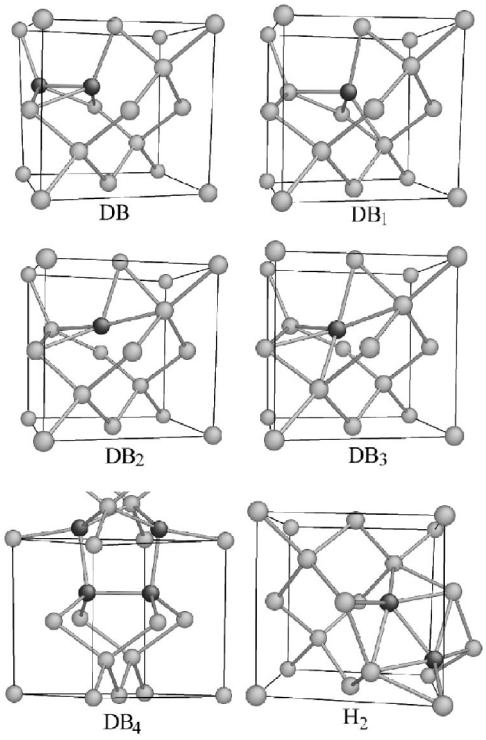

FIG. 3. Interstitials generated by random placement and subsequent relaxation using EDIP. The corners of a diamond unit cell are connected by lines, and atoms occupying interstitial positions are darkened. Bonds are drawn between atoms closer than 2.56 Å. H_2 involves two atoms which are extra to the diamond unit cell—all other defects pictured here involve only one extra atom.

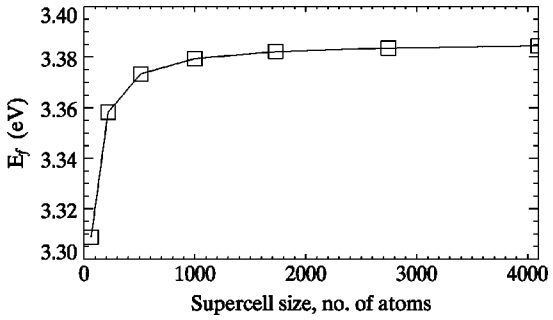

FIG. 4. Formation energy for ⟨110⟩ dumbell calculated in various sized supercells with periodic boundary conditions.

tion energy and formation volume of which are 2.38 eV and +1.1 Å^3, respectively. This defect has been studied numerous times under various names. We adopt the latest nomenclature for this defect: the fourfold coordinated defect (FFCD).[53] The (FFCD) is pictured in Fig. 6.

The earliest (to our knowledge) descriptions of this defect were by Stillinger and Weber,[9] and by Wooten, Winer, and Weaire,[54] who used it to generate samples of amorphous Si. Later, Motooka[55] described how a divacancy/di-interstitial complex results in an equivalent configuration. Tang *et al.*[56] later rediscovered this arrangement as the result of the close approach of a vacancy-interstitial pair, and made a tight-binding calculation of the formation energy (3.51 eV). Stock *et al.*[57] identified the Stillinger and Weber bond defect, the WWW bond-switching mechanism, and the Tang "*I-V* complex" as one and the same. Cargoni *et al.*[58] examined the bond defect with tight-binding molecular dynamics (TBMD) and *ab initio* Hartree-Fock calculations, reporting a formation energy of 3.26 eV. Marques *et al.*[50] used the Tersoff 3 (T3) potential[11] to calculate a formation energy of 3.01 eV. Recently, Goedecker *et al.*[53] used density functional theory (DFT) to calculate the formation energy of this defect. The local density approximation (LDA) predicted 2.34 eV, and the general gradient approximation (GGA) predicted 2.42 eV. These latest *ab initio* calculations are in remarkable agreement with EDIP.

It is interesting to note that while the formation energy of this defect is dramatically lower than that of the other defects present in our samples, it does not occur in any of them. This

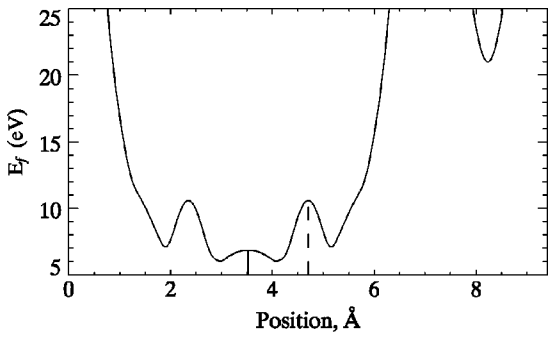

FIG. 5. Unrelaxed formation energy for an interstitial placed along the unit cell body diagonal in Si, calculated using EDIP. The solid and dashed vertical lines indicate the positions of the hexagonal and tetragonal interstials, respectively.

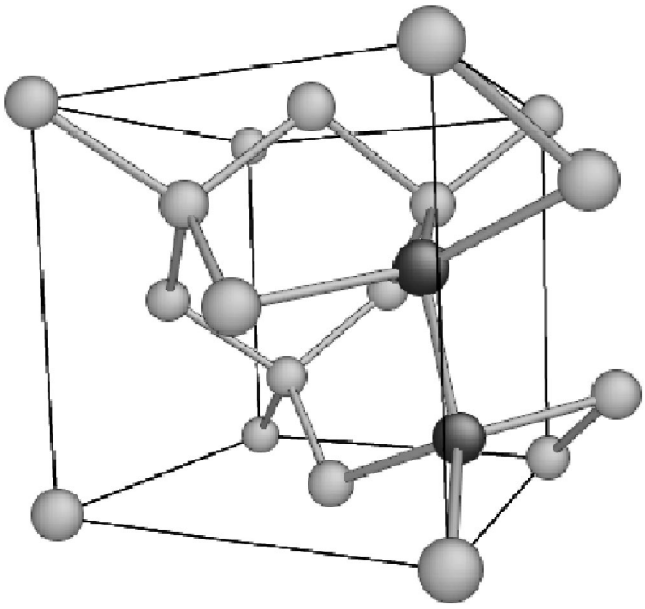

FIG. 6. The fourfold coordinated defect referred to a unit cell. The two displaced atoms are darkened.

is perhaps due to the orchestrated movement of atoms that is required to produce it, which decreases the likelihood of it naturally occuring.

Three types of divacancies cropped up in the samples with random vacancy placement. One involved missing nearest neighbors (V_{2N}) with symmetric outward breathing. Another involved missing next-nearest neighbors (V_{2NN}). The third also consisted of missing next-nearest neighbors, but differed in that the common neighbor to the two vacant sites shifted to become threefold coordinated (V_{2a}). When isolated in a supercell, V_{2a} survived annealing, but V_{2NN} relaxed into a fourth configuration, V_{2NNr}, involving missing nearest neighbors that differed from V_{2N} in that instead of involving six threefold coordinated atoms, it had only three threefold coordinated atoms accompanied by a single fivefold coordinated atom. These vacancy configurations are illustrated in Fig. 7. Though one case of the divacancy V_{2NN} had survived the annealing step in one of the random-placement samples, it was not in isolation in the supercell, and the strain fields of the other defects present may have served to stabilize it to some degree.

The relaxed monovacancy and divacancy energies show good qualitative agreement with DFT/LDA calculations, which predict 3.29, 4.63, and 5.90 eV for V, V_{2N}, and V_{2NN}, respectively.[59] The binding energy for the divacancy is therefore 1.60 and 1.95 eV according to EDIP and DFT/LDA, respectively. We note that while the monovacancy, "simple" divacancy, and "split" divacancy of Seong *et al.*[59] have the same unrelaxed structures as V, V_{2N}, and V_{2NN}, respectively, the energies we cite here are for the relaxed structures, on which DFT/LDA and EDIP differ. In the case of V, for example, Seong *et al.* report a monovacancy structure that is somewhere between the symmetric V favored by EDIP and the distorted V_{JT}.

The formation volume for an isolated vacancy was found to be +28.8 Å^3. The EDIP monovacancy is therefore

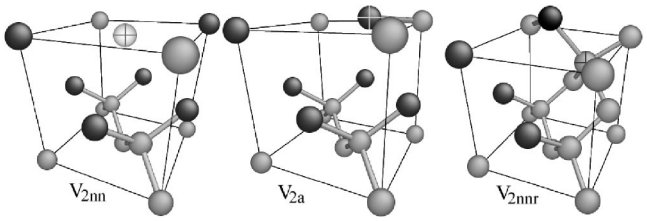

FIG. 7. Divacancy complexes referred to a unit cell (left to right): V_{2NN}, V_{2a}, and V_{2NNr}. Highlighted and darkened atoms are twofold and threefold coordinated, respectively. At left, two next-nearest neighbors are missing from the upper half of the unit cell. At center, the twofold coordinated atom (marked with a cross) has broken symmetry and become threefold coordinated. Annealing V_{2NN} at room temperature yielded the rightmost figure, in which the uppermost atom (black) is fivefold coordinated. This atom is not part of the unit cell shown, but is included to provide context. While V_{2NNr} was generated by annealing V_{2NN}, it actually involved missing nearest neighbors, similar to the simpler V_{2N} (not shown).

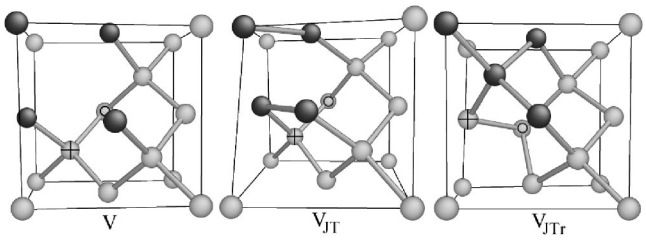

FIG. 8. Stable EDIP monovacancy configurations. At left is the outward-breathing vacancy (V) observed in all randomly generated samples. Vacancy neighbors are darkened. The Jahn-Teller distortion with bonding between pairs of vacancy neighbors is shown at center (V_{JT}), and the result upon a room temperature annealing of this defect is shown at right ($V_{\mathrm{JT}r}$). The cross marks an atom whose position changes significantly between the three configurations shown, as does the circle. $V_{\mathrm{JT}r}$ contains one five-coordinated atom (circle) and non three-coordinated atom (back lower left corner).

outward-breathing (the atomic volume of the EDIP crystal is 20.0 Å^3, in agreement with early *ab initio* calculations.[60,61] Later calculations have predicted an inward-breathing vacancy,[59,62,63] and a recent DFT/LDA calculation study showed that the relaxation around a neutral monovacancy has a formation volume of −1.7 Å^3.[64] The negative formation volume accompanied a Jahn-Teller distortion in which the neighbors of the vacant site bond pairwise across ⟨110⟩ directions. While we found that that such a defect is stable using EDIP (and it did indeed have a negative formation volume of −14.5 Å^3), its formation energy was higher than that of the monovacancy: 4.06 eV. When comparing formation volumes of various defects, it is helpful to remember that the unrelaxed vacancy has a formation volume of +20 Å^3, whereas that of an unrelaxed monointerstitial configuration is −20 Å^3. A negative formation volume, therefore, is not as surprising for an interstitial as for a vacancy, where relaxation must be very significant to pack atoms more efficiently than the crystal.

The defect (V_{JT}) disappeared upon annealing at 300 K for 500 ps in three samples we tested, evolving each time into a defect ($V_{\mathrm{JT}r}$) involving one three-coordinated and one five-coordinated atom and having a formation energy and volume of 3 eV and −6.7 Å^3, respectively. We calculated the effect of both V_{JT} and $V_{\mathrm{JT}r}$ on the elastic constants at 0 K. Whereas the monovacancy V is seen to cause a reduction in every elastic constant, the other two monovacancy types show behavior similar to the FFCD in that they actually stiffen C_{12} and the bulk modulus. In each case, however, the Young's modulus is observed to lessen. The three monovacancy configurations are illustrated in Fig. 8. The comparison of $V_{\mathrm{JT}r}$ with V_{2NNr} reveals a common structure: each has a fivefold coordinated atom with four bonds almost being coplanar, and the fifth bond pointing in the general direction of the threefold coordinated atoms (this is not particularly evident in Figs. 7 and 8—only two of the almost coplanar bonds are shown in each case).

The results for formation energy, formation volume, and effects on elastic constants of the isolated defect samples are summarized in Table VI. While the sign on the deviation from crystalline elastic constants varied between vacancies and interstitials in some cases (C_{12} and B), all defects were observed to reduce Young's modulus. When taken on a per-atom basis, the effect on the ⟨100⟩ Young's modulus is quite similar among all defect types presented in Table VI, being bracketed between −0.25 and −0.45% (aside from the tetrahedral interstitial, which is locally unstable according to both EDIP and LDA calculations).

While one might expect that greater formation volume magnitude would be accompanied by a larger formation energy (due to larger strain fields), we found that the relationship between formation volume and and formation energy among defects was not completely rigid. The two defects with the lowest formation energies, H_2 and the FFCD, did indeed have low formation volume magnitudes. The relationship between V_{2N} and V_{2NNr}, however, is the opposite of what one would expect, as is the large formation volume that accompanies the most stable monovacancy V. One may also wonder if the overall positive formation volume may not be driving the decrease in elastic modulus. This is clearly not the case, as can be seen by considering Table VI. For every type of point defect, having positive or negative formation volume, the change in Young's modulus is negative. The changes in other elastic constants are also uncorrelated with formation volume. This is to be expected, since elastic constants are not strictly a function of volume, but also of bonding topology and bond strength.

We examined the changes in ring structure that accompanied the defects of Table VI in an attempt to relate ring statistics and coordination numbers to the observed changes in elastic constants. The interstitial defects which involved extra atoms did not present any obvious pattern in this regard, but the vacancy defects did. Table VII shows the ring and coordination figures for the vacancy and FFCD defects. A ring is defined here as a closed path which is a series of sequentially bonded atoms without overlap, and a primitive ring is a ring which cannot be decomposed into two smaller rings.[65,66] We determined primitive ring statistics using a recent effective ring search algorithm.[65]

It can be seen that with increased numbers of undercoordinated atoms, the bulk modulus is lessened. Concurrent

TABLE VI. Formation energies, volumes, and percent change in elastic constants for a single defect in a 1728-atom supercell, calculated using EDIP. The numbers in parenthesis represent how many of the 90 "extra" atoms randomly inserted into our samples appeared in a particular interstitial type. The number of vacant sites appearing in a particular vacancy complex is also shown in parenthesis, also out of a total of 90.

	E_f, (eV)			V_f, Å^3							
	EDIP	LDA	GGA	EDIP	LDA	C_{11}	C_{12}	C_{44}	B	$E_{\langle 100\rangle}$	$E_{\langle 110\rangle}$
DB	3.38 (67)	2.88[a]	3.31[a]	8.7	−2.0[b]	−0.02	0.72	−0.32	0.29	−0.35	−0.25
DB_1	3.55 (4)			7.0		−0.04	0.64	−0.35	0.25	−0.28	−0.27
DB_2	3.55 (4)			6.7		−0.10	0.59	−0.38	0.20	−0.41	−0.31
DB_3	3.53 (6)			6.2		−0.03	0.54	−0.40	0.22	−0.35	−0.28
DB_4	3.50 (1)			−0.6		−0.03	0.56	−0.36	0.22	−0.29	−0.26
Tet	4.10 (0)	3.43[c]	4.07[c]	19.6		0.12	0.81	−0.43	0.41	−0.18	−0.24
Hex	4.19 (0)	2.87[a]	3.31[a]	8.3		−0.11	0.50	−0.45	0.16	−0.38	−0.35
Hex_A	3.95 (0)			7.4		−0.10	0.63	−0.50	0.21	−0.42	−0.38
FFCD	2.38 (0)	2.34[a]	2.42[a]	1.1	5.9[b]	−0.12	0.18	−0.31	0.01	−0.26	−0.25
H_2	4.81 (8)			−4.0		−0.09	1.00	−0.42	0.43	−0.58	−0.36
V	3.22 (84)	3.29[d]		28.8	12.8[d]	−0.31	−0.42	−0.27	−0.34	−0.26	−0.28
V_{JT}	4.06 (0)	3.49[e]		−14.5	−1.7[e]	−0.21	0.32	−0.44	0.03	−0.45	−0.38
V_{JTr}	3.65 (0)			−6.7		−0.18	0.24	−0.32	0.01	−0.37	−0.29
V_{2N}	4.84 (2)	4.63[d]		53.4	16.3[d]	−0.54	−0.61	−0.46	−0.55	−0.50	−0.49
V_{2NN}	6.77 (2)	5.90[d]		51.3	14.1[d]	−0.67	−0.81	−0.57	−0.72	−0.61	−0.60
V_{2NNr}	5.23 (0)			16.2		−0.38	0.05	−0.50	−0.18	−0.57	−0.48
V_{2a}	5.84 (2)			47.6		−0.61	−0.75	−0.58	−0.65	−0.54	−0.58

[a]From Ref. 53.
[b]From Ref. 56.
[c]From Ref. 51.
[d]From Ref. 59.
[e]From Ref. 64.

with this trend are the softening effects of the loss of six-rings and the gain of larger rings. Offsetting factors include the gain of overcoordinated atoms and rings of size less than 6. The relationship between coordination, ring size population, and bulk modulus was more complicated for many of the defects not shown in Table VII, but the greatest stiffening of the bulk modulus did coincide with the H_2 and tet defects, which were characterized by overcoordinated atoms and small rings. The numbers for these other defects are shown in Table VIII. The hex and hex_A defects would appear to be likely to raise the bulk modulus more than other defects above them in Table VIII, given their three-rings and their lack of large rings, but perhaps their peculiar planar geometry partially nullifies these stiffening characteristics.

It it interesting to note that while EDIP may have erred in predicting hex_A to have a lower formation energy than hex, the effects on the supercell elastic constants are much the same in either case. The ordering of the formation energies of the tetrahedral and the hex_A interstitials agrees with LDA calculations,[51] while this was not the case with the symmetric hexagonal interstitial.

Finally, we used the numbers in Table VI to predict the results for the samples (summarized in Fig. 1) generated by random defect placement. We compared the elastic constant changes in these samples to the sum of the individual contributions listed in Table VI for the defects involved. This sum usually overestimated the change in elastic constants, making the worst approximation for the samples containing the highest defect concentration. The error was in some cases as high as 33%, but averaged only 10%. The accumulation of elastic constant changes was therefore nearly linear with increasing defect content, as was shown in Fig. 1, though some saturation effects are understandably present at such high defect concentrations.

IV. DISCUSSION

A. Defects and elasticity

We have used a well tested, physically motivated potential to study the effects of defects on the elastic constants of silicon. That our results contradict those of Clark and Ackland[32] is not surprising, in view of the untested potential they used and the lack of essential physics, such as explicit angular dependence. The elastic constants of the CA potential are significantly different from experiment, even more than the authors may have realized. They appear to have mistakenly used the experimental constants of Si at 1477 K as a reference for their calculations at 0 K.[32,37] The elastic constants of the CA potential differ from experiment[38] by 11,

TABLE VII. Coordination and ring statistics changes compared to the percent change in bulk modulus for vacancy defects and the FFCD. Net changes are for isolated defects in a 1728-atom supercell, referred to a similar crystalline supercell. The net change in the number of atoms having a particular coordination is given by *N*. The numbers under the "rings" heading refer to the net gain or loss of rings of a particular size.

	N			Rings							
Defect	2	3	5	5	6	7	9	11	12	14	ΔB, %
V_{JT}	0	0	0	4	−12	0	4	0	0	0	0.03
FFCD	0	0	0	4	−12	8	0	0	0	0	0.01
$V_{\mathrm{JT}r}$	0	1	1	4	−10	0	2	0	0	0	0.01
V_{2NNr}	0	3	1	4	−16	0	0	2	0	0	−0.18
V	0	4	0	0	−12	0	0	0	4	0	−0.34
V_{2N}	0	6	0	0	−18	0	0	0	2	9	−0.55
V_{2a}	0	6	0	2	−22	0	0	0	7	0	−0.65
V_{2NN}	1	6	0	0	−22	0	0	0	8	0	−0.72

91, and 67 %, for C_{11}, C_{12}, and C_{44}, respectively. The disagreement in results is perhaps best summarized by considering Young's modulus, which is commonly of importance in practical situations. We observed that all defect types, whether isolated or in random arrangements, caused a lessening of Young's modulus, whereas the results of Clark and Ackland imply that the presence of vacancies or interstitials causes Young's modulus to increase.

The only other study of the effects of defects on elastic constants that we were able to find in the literature was the tight-binding molecular dynamics work of De Sandre *et al.*[45] It is difficult to compare our findings with regard to point defects with those of that study given that the lowest concentration considered there was 9.3%, at which point the crystal-to-amorphous transition has begun.[67] Nevertheless, the authors report "the evolution of the elastic constants towards an overall softening during the crystal-to-amorphous transition."

Our results also qualitatively agree with the experimental data available in the literature. Burnett and Briggs made measurements of the elastic constants of silicon which had been bombarded with arsenic and silicon ions.[1] Their samples varied from being near the amorphization threshold to being completely amorphized, but in every case, both C_{11} and C_{44} decreased as the radiation damage increased.

As an additional check on our results, we created more defect-containing simulation cells using the Stillinger-Weber (SW) potential[9] as we had done with EDIP in Sec. II A 1. One set of cells contained vacancies, the other interstitials, both in varying concentrations as in Fig. 1. In each case, the Young's modulus along ⟨110⟩ and ⟨100⟩ decreased with increasing defect content. Furthermore, an SW simulation of the isolated defects *V*, DB, and tet, as in Table VI, predicted a decrease in both $E_{\langle 100\rangle}$ and $E_{\langle 110\rangle}$ in all three cases. Corroboration by the most widely used potential for silicon suggests that our general conclusion is robust.

Since it would appear from Table III that, even at the high defect concentrations studied here, point defects have an effect on the elastic constants that is fairly independent of one another, the details of coordination within each defect as it relates to connectivity in the lattice appears to be important. As shown in Table VI, a vacancy will have different effects on the elastic constants depending on its relaxed bonding configuration. While EDIP does (by design) produce elastic constants for silicon close to those of experiment, the configurations of relaxed point defects it produces do not correspond precisely with those predicted by *ab initio* calculations.

TABLE VIII. Coordination and ring statistics changes compared to the percent change in bulk modulus for interstitial defects, as in Table VII.

	N		Rings					
Defect	5	6	3	4	5	6	7	ΔB, %
H_2	8	0	6	0	2	−2	0	0.43
Tet	4	0	0	6	0	0	0	0.41
DB	2	0	2	0	0	0	2	0.29
DB_1	2	0	2	0	1	−4	4	0.25
DB_4	2	0	0	1	8	−12	8	0.22
DB_3	4	0	3	1	0	−2	3	0.22
Hex_A	6	1	6	0	0	5	0	0.21
DB_2	2	0	2	0	1	−4	3	0.20
Hex	6	1	6	0	0	5	0	0.16

We should mention that the volume expansion shown in Fig. 2 for EDIP is likely not in good agreement with reality, since the samples involved contained mostly monovacancies, which were shown here to be outward breathing in EDIP. As noted above, recent *ab initio* calculations predict the the monovacancy to have a negative formation volume, which would correspond to a densification with increasing monovacancy content. We must therefore be cautious as to which results presented here we expect to correspond to reality.

This word of caution does not preclude two generalizations of practical interest, however. We reiterate that the general trend of Young's modulus is consistently downward with increasing defect content, regardless of the positive or negative formation volume of the defects involved. This effect varies within a very narrow range for the defect configurations considered here. It should therefore be possible to make reasonable predictions of the shift in the Young's modulus of a radiation-damaged silicon sample in which isolated point defects dominate, even if the exact geometry of each point defect is not well known. The calculation presented here of the crystalline/amorphous composite sample is also encouraging. It appears that a reasonable prediction of changes in Young's modulus can also be made for radiation-damaged samples in which amorphous regions are important, based simply on the volume fraction of amorphous material, according to Eq. (9).

B. Interatomic potentials

There are advantages to using an empirical potential, instead of *ab initio* methods, for the work presented here. The

first is that since empirical potentials will always be computationally cheaper than *ab initio* calculations, it is important to continue the development and characterization of such potentials in order to enable the study of systems many times the size of those accessible to *ab initio* methods. Secondly, despite the fact that powerful computers could perform *ab initio* calculations on the 1728 atom cells (the largest we considered), the large number of such cells and the demands of the numerous annealing steps involved in the preparation of our simulation cells would have been impractical. We prepared over 60 cells containing 1728 atoms, each one requiring more than 250 K computational steps for the preparation alone. The use of an empirical potential allowed us to compile statistics on the effects of random defect arrangements and notice trends, something that would not have been possible using *ab initio* methods.

We briefly discuss what our results might imply about the physics of covalent bonding. The fact that we get qualitatively similar results with EDIP and SW, which differ sharply with CA, confirms the common wisdom that angular forces are present in covalent solids, as argued by Born almost a century ago. The pairwise repulsion of first neighbors in the CA potential, similar to the early potential of Pearson *et al.*[68] [which also does not perform as well as SW (Ref. 29)], is not equivalent to an explicit angular force.

For the reasons mentioned in the introduction, however, the reasonable results of SW for defects are quite surprising because the potential can only be justified for weakly distorted, rigid sp^3 hybrids. There is no question that both the bond order[26] and the strength of angular forces[12] depend on the local atomic environment, as also implied by analytical approximations of tight-binding models.[28] EDIP attempts to capture these effects with only a simple scalar, the coordination number. Of course, this precludes the possibility of gradual rehybridization under shear, before changes in bonding topology occur, and it seems this is related to the underestimate of C_{44} for both crystal and amorphous structures. The SW potential misses all of this physics, and yet somehow manages to describe defect configrations fairly well. The fortuitous reason may be that the "optimal" angular function for silicon, obtained by inversion of *ab initio* cohesive energy curves for silicon, neglecting environment dependence, happens to match the SW angular term quite well.[26]

In any case, it is clear that any potential for silicon must take into account the local atomic environment, if not explicitly, as in EDIP, then at least implicitly by considering all neighboring atoms, as in SW and Tersoff. The CA potential, similar to the Ackland potentials before it,[34,35] makes the *ad hoc* assumption of four diamond-like bonds per atom, which surely does not apply to most defects. Ackland acknowledged the need for coordination dependence in his original paper,[34] by increasing the bond order for undercoordinated atoms ($Z=3$), albeit to a value inappropriate for *ab initio* graphitic silicon;[26] however, this modification was not included in the CA potential.[32] The significant decrease in bond order of roughly $Z^{-1/2}$ for overcoordination ($Z>4$)[12,26] was also neglected, so the different conclusion regarding the effect of point defects on elastic constants versus the present study can be attributed to an inadequate description of covalent bonding.

V. CONCLUSIONS

We have characterized the structure of various point defects according to EDIP and calculated their individual effects on elastic constants. We have shown that, in general, the elastic constants of silicon vary with defect concentration in a roughly linear fashion at defect concentrations up to 0.3%. We have also demonstrated the effects of an amorphous region embedded in a crystalline supercell to be well described by a simple equation involving the volume fraction of amorphous material. We have also calculated elastic constants for several amorphous samples, and concluded that, in spite of a good overall description of the amorphous phase, EDIP consistently underestimates C_{44}. As in the case of the crystal, this may be due to its neglect of rehybridization under strain (as in SW).

The defect structures and formation energies predicted by the potential, such as the energetically favored fourfold coordinated defect, seem fairly realistic, so we may place some confidence in their effects on elasticity. We predict that both interstitial and vacancy defects, singly and in random combination, lessen the Young's modulus of silicon. We also find that the individual contributions of various defect types to changes in Young's modulus are confined to a surprisingly small range. These appear to be robust conclusions for potentials taking into account explicit angular forces for covalent bonds.

ACNOWLEDGMENT

Support for this research came from the Charles Stark Draper Laboratory, the Cambridge-MIT Institute, and the United States Department of Energy, Basic Energy Science, under Grant No. DE-FG02-89ER45396. The views expressed in this article are those of the author and do not reflect the official policy or position of the United States Air Force, Department of Defense, or the U.S. government.

*Electronic address: hobbs@mit.edu

[1] P. J. Burnett and G. A. D. Briggs, J. Mater. Sci. **21**, 1828 (1986).
[2] M. Szabadi, P. Hess, A. J. Kellock, H. Coufal, and J. E. E. Baglin, Phys. Rev. B **58**, 8941 (1998).
[3] X. Zhang, J. D. Comins, A. G. Every, P. R. Stoddart, W. Pang, and T. E. Derry, Phys. Rev. B **58**, 13 677 (1998).
[4] R. Bhadra, J. Pearson, P. Okamoto, L. Rehn, and M. Grimsditch, Phys. Rev. B **38**, 12 656 (1988).
[5] M.-J. Caturla, T. Diaz de la Rubia, L. A. Marques, and G. H. Gilmer, Phys. Rev. B **54**, 16 683 (1996).
[6] K. Nordlund and R. S. Averback, Phys. Rev. B **56**, 2421 (1997).
[7] K. Nordlund, M. Ghaly, R. S. Averback, M. Caturla, T. Diaz de la

Rubia, and J. Tarus, Phys. Rev. B **57**, 7556 (1998).
[8] J. Nord, K. Nordlund, and J. Keinonen, Phys. Rev. B **65**, 165329 (2002).
[9] F. H. Stillinger and T. A. Weber, Phys. Rev. B **31**, 5262 (1985).
[10] J. Tersoff, Phys. Rev. B **37**, 6991 (1988).
[11] J. Tersoff, Phys. Rev. B **38**, 9902 (1988).
[12] M. Z. Bazant, E. Kaxiras, and J. F. Justo, Phys. Rev. B **56**, 8542 (1997).
[13] J. F. Justo, M. Z. Bazant, E. Kaxiras, V. V. Bulatov, and S. Yip, Phys. Rev. B **58**, 2539 (1998).
[14] M. de Koning, A. Antonelli, M. Z. Bazant, E. Kaxiras, and J. F. Justo, Phys. Rev. B **58**, 12 555 (1998).
[15] S. Goedecker, F. Lancon, and T. Deutsch, Phys. Rev. B **64**, 161102 (2001).
[16] S. Balboni, E. Albertazzi, M. Bianconi, and G. Lulli, Phys. Rev. B **66**, 045202 (2002).
[17] C. R. Miranda, R. W. Nunes, and A. Antonelli, Phys. Rev. B **67**, 235201 (2003).
[18] M. Prasad and T. Sinno, Phys. Rev. B **68**, 045207 (2003).
[19] I. Pizzagalli, P. Beauchamp, and J. Rabier, Philos. Mag. **83**, 1191 (2003).
[20] N. Bernstein, M. J. Aziz, and E. Kaxiras, Phys. Rev. B **61**, 6696 (2000).
[21] S. M. Nakhmanson and D. A. Drabold, J. Non-Cryst. Solids **266**, 156 (2000).
[22] L. Brambilla, L. Colombo, V. Rosato, and F. Cleri, Appl. Phys. Lett. **77**, 2337 (2000).
[23] G. Hadjisavvas, G. Kopidakis, and P. C. Kelires, Phys. Rev. B **64**, 125413 (2001).
[24] S. M. Nakhmanson and N. Mousseau, J. Phys.: Condens. Matter **14**, 6627 (2002).
[25] P. Keblinski, M. Z. Bazant, R. K. Dash, and M. M. Treacy, Phys. Rev. B **66**, 064104 (2002).
[26] M. Z. Bazant and E. Kaxiras, Phys. Rev. Lett. **77**, 4370 (1996).
[27] M. Z. Bazant, Ph.D. thesis, Harvard University, 1997.
[28] D. G. Pettifor and I. I. Oleinik, Phys. Rev. Lett. **84**, 4124 (2000).
[29] H. Balamane, T. Halicioglu, and W. A. Tiller, Phys. Rev. B **46**, 2250 (1992).
[30] A. Witvrouw and F. Spaepen, J. Appl. Phys. **74**, 7154 (1993).
[31] S. I. Tan, B. S. Berry, and B. L. Crowder, Appl. Phys. Lett. **20**, 88 (1972).
[32] S. J. Clark and G. J. Ackland, Phys. Rev. B **48**, 10 899 (1993).
[33] P. Alinaghian, S. R. Nishitani, and D. G. Pettifor, Philos. Mag. B **69**, 889 (1994).
[34] G. Ackland, Phys. Rev. B **40**, 10 351 (1989).
[35] G. J. Ackland, Phys. Rev. B **44**, 3900 (1991).
[36] M. Karimi, H. Yates, J. R. Ray, T. Kaplan, and M. Mostoller, Phys. Rev. B **58**, 6019 (1998).
[37] M. D. Kluge, J. R. Ray, and A. Rahman, J. Chem. Phys. **85**, 4028 (1986).
[38] J. J. Hall, Phys. Rev. **161**, 756 (1967).
[39] T. R. Forester and W. Smith, *The DL_POLY_2 Reference Manual*, CCLRC, Daresbury Laboratory, Daresbury, Warrington WA4 4AD, England, 2001, http://www.dl.ac.uk/TCSC/Software/DL_POLY/
[40] J. F. Nye, *Physical Properties of Crystals* (Oxford University Press, Oxford, 1985).
[41] C. S. G. Cousins, L. Gerward, J. S. Olsen, B. Selmsmark, and B. J. Sheldon, J. Appl. Crystallogr. **15**, 154 (1982).
[42] F. R. S. Hearmon, *An Introduction to Applied Anisotropic Elasticity* (Oxford University Press, London, 1961).
[43] M. G. Ashby and D. R. H. Jones, *Engineering Materials 1: An Introduction to Their Properties & Applications* (Butterworth-Heinemann, Oxford, 1996).
[44] J. S. Custer, M. O. Thompson, D. C. Jacobson, J. M. Poate, S. Roorda, W. C. Sinke, and F. Spaepen, Appl. Phys. Lett. **64**, 437 (1994).
[45] G. De Sandre, L. Colombo, and C. Bottani, Phys. Rev. B **54**, 11 857 (1996).
[46] G. Servalli and L. Colombo, as discussed in De Sandre *et al.* (45).
[47] X. Jiang, M. Wang, K. Schmidt, E. Dunlop, J. Haupt, and W. Gissler, J. Appl. Phys. **69**, 3053 (1991).
[48] J. Zuk, H. Kiefte, and M. J. Clouter, J. Appl. Phys. **73**, 4951 (1993).
[49] R. L. C. Vink, G. T. Barkema, W. F. van der Weg, and N. Mousseau, J. Non-Cryst. Solids **282**, 248 (2001).
[50] L. A. Marques, L. Pelaz, J. Hernandez, J. Barbolla, and G. H. Gilmer, Phys. Rev. B **64**, 045214 (2001).
[51] W.-K. Leung, R. J. Needs, G. Rajagopal, S. Itoh, and S. Ihara, Phys. Rev. Lett. **83**, 2351 (1999).
[52] S. J. Clark and G. J. Ackland, Phys. Rev. B **56**, 47 (1997).
[53] S. Goedecker, T. Deutsch, and L. Billard, Phys. Rev. Lett. **88**, 235501 (2002).
[54] F. Wooten, K. Winer, and D. Weaire, Phys. Rev. Lett. **54**, 1392 (1985).
[55] T. Motooka, Phys. Rev. B **49**, 16 367 (1994).
[56] M. Tang, L. Colombo, J. Zhu, and T. Diaz de la Rubia, Phys. Rev. B **55**, 14 279 (1997).
[57] D. M. Stock, B. Weber, and K. Gartner, Phys. Rev. B **61**, 8150 (2000).
[58] F. Cargnoni, C. Gatti, and L. Colombo, Phys. Rev. B **57**, 170 (1998).
[59] H. Seong and L. J. Lewis, Phys. Rev. B **53**, 9791 (1996).
[60] M. Scheffler, J. P. Vigneron, and G. B. Bachelet, Phys. Rev. B **31**, 6541 (1985).
[61] U. Lindefelt, Phys. Rev. B **28**, 4510 (1983).
[62] P. J. Kelly and R. Car, Phys. Rev. B **45**, 6543 (1992).
[63] A. Antonelli and J. Bernholc, Phys. Rev. B **40**, 10 643 (1989).
[64] A. Antonelli, E. Kaxiras, and D. J. Chadi, Phys. Rev. Lett. **81**, 2088 (1998).
[65] X. Yuan and A. N. Cormack, Comput. Mater. Sci. **24**, 327 (2002).
[66] C. S. Marians and L. W. Hobbs, J. Non-Cryst. Solids **124**, 242 (1990).
[67] L. Colombo and D. Maric, Europhys. Lett. **29**, 623 (1995).
[68] E. M. Pearson, T. Takai, T. Halicioglu, and W. A. Tiller, J. Cryst. Growth **70**, 33 (1984).